Vol 2 (2) (2021)

MCA

Measurement, control and automation

Website: https:// mca-journal.org

ISSN 1859-0551

T-type based Grid-Side Converter Control Design of Double Fed Induction Generator – A practical approach

Manh Linh Nguyen[1*], Van Sy Vu [1] and Van Vu Tong[1]

[1] *Hanoi University of Science and Technology, VietNam*

[*] *Corresponding author E-mail: linh.nguyenmanh@hust.edu.vn*

Abstract

In this paper, the control design for the grid-connected converter used as a part of the wind turbine generator is discussed. First, the three-phase T-type multilevel converter, which exhibits several advantages such as low total harmonic distortion, reduced voltage stress, and switching loss, is employed for the power stage. Second, finite control set model predictive control (FCS-MPC) is adopted to achieve a multi-objective optimization solution for the inner grid-connected current control loop. This approach not only allows the current to quickly track its desired value but also minimizes the capacitor voltage balance and the switching loss. Finally, a practical approach is proposed to design the Fuzzy-based PI controller for the DC bus voltage regulation. The design procedure is straightforward, and only requires several known information getting from the converter. Specifically, the proposed controller allows users to exactly restrict the inrush current, as well as minimize the overshoot of the DC bus voltage during startup. The effectiveness of the proposed control strategy is verified by numerical simulations. In which all controlled algorithms are implemented by standard C language such that the consistency between simulations and future practical implementations is guaranteed.

Keywords: *Double-fed induction generator; Grid-connected converter; Model predictive control; Fuzzy logic control; PI control.*

Symbols

Abbreviations

THD	Total Harmonic Distortion
FCS-MPC	Finite Control Set-Model Predictive Control
PI	Proportional Integral
EMI	Electromagnetic Interference
FC	Flying Capacitor
NPC	Neutral Point Clamp
CHB	Cascade H-Bridge
DFIG	Double-Fed Induction Generator
FLC	Fuzzy Logic Control
2L	Two-Level
3L	Three-Level

Tóm tắt

Bài báo này thảo luận về một cách tiếp cận mới trong thiết kế bộ biến đổi phía lưới sử dụng trong hệ thống tua-bin gió. Đầu tiên, cấu trúc hình T đa mức với những ưu điểm nổi trội như giảm điện áp rơi trên van, độ méo sóng hài thấp, và giảm tần số chuyển mạch được lựa chọn làm mạch lực.Tiếp theo, mạch vòng dòng điện sử dụng chiến lược điều khiển dự báo tựa mô hình để giải quyết đồng thời nhiều yêu cầu của mạch vòng dòng điện như cân bằng điện áp trên tụ và giảm tổn hao chuyển mạch song song với việc đưa dòng điện bám với giá trị đặt. Cuối cùng, một cách tiếp cận thực tế được đề xuất để thiết kế bộ điều khiển điện áp DC bus sử dụng kết hợp bộ điều khiển PI truyền thống kết hợp với logic mờ.Ngoài ra, phương pháp được đề xuất còn có thể hạn chế dòng điện khởi động cùng với đó là giảm độ quá điều chỉnh của điện áp DC bus.Tính hiệu quả của phương pháp được đề xuất được kiểm chứng bằng mô phỏng. Trong đó thuật toán điều khiển được lập trình hoàn toàn bằng ngôn ngữ C, điều này giúp khẳng định tính nhất quán giữa mô phỏng và thực nghiệm sau này.

1. Introduction

During the last decades, along with the increasing human demand and the depletion of fossil energies, renewable energy is known as an effective solution to solve the global energy problem. Besides the solar energy, wind energy accounts for a large proportion and continues to grow at a rapid pace. To effectively utilize energy from the wind, the generator and the converter need to use in the best efficiency. The wind turbine system falls in two types: fixed speed and variable speed. Owing to the benefit of operational and economic over fixed wind turbine such as higher performance and power quality, wide power adjustment range, reduced mechanical load and stress..., the variable wind turbine systems are preferred in application with high power [1].There are two types of variable wind turbine: DFIG wind turbines and direct-in-line wind turbines. In which, DFIG wind turbines are often used more than direct-in-line wind turbines in recent wind power application. The general structure of the DFIG system includes: the rotor terminal is

Received: 10 January 2022; Accepted: 14 March 2022.

coupled to the shaft of the wind turbine through a gearbox and connected to the grid by a back-to-back converter, the stator terminal is connected directly to the grid [2].

The main advantage of DFIG is that the semiconductor switches only have to transmit a part of system's power. The back-to-back converter typically accounts for about 30% of a system's total transmission power. This means that the power loss on the semiconductor switches is reduced, and the size of the converter is also smaller so provide higher efficiency and reliability. In return, the control system becomes more complicated to handle problems such as starting, synchronization, and oscillatory transients [3]. Therefore, studying on control of back-to-back converter has attracted great attention [4–7].

A conventional back-to-back converter is an AC-DC-AC converter, with the classic structure, it's usually composed of two three-phase bridge converters and has been widely used in practical applications. To further enhance the performance of this converter in term THD, switching loss, dv/dt, voltage stress, electromagnetic interference (EMI), etc., multi-level topologies emerge as an alternative to the traditional ones [8]. There are several multi-level topologies that can be used for back-to-back converters, such as flying capacitor (FC), neutral point clamped (NPC), cascade H-bridge (CHB). Each topology has its own advantages and disadvantages. For the CHB topology, an arbitrary number of voltage level can made, thus making the output voltage more sinusoidal. However, the most obvious disadvantage is the need for multiple isolated DC sources, which are usually only available in solar power conversion [9]. The NPC topology, which is also called diode clamp topology, only requires a DC power supply like a two-level inverter but gives better performance. However, increasing the number of levels of NPC not only makes the circuit structure more complex, but also makes the DC link voltage control more difficult. Therefore, this topology is often used for 3-level converters. The T-type converter is one of the advanced NPCs topologies with the advantages of fewer switching elements and higher efficiency [10]. This research focuses on the control strategy for the T-type converter in grid-connected mode, as a part of the DFIG system.

In general, the control scheme of a grid-side converter is classified into two cascade loops. The inner loop is the current regulator which plays the most important role in the power transfer process [11]. In addition, strictly requirements of the grid code such as sinusoidal current with satisfactory total harmonic distortion (THD) is mainly governed by this control loop [12]. The outer loop regulates the DC link voltage by balancing the power exchange between the grid-side and the rotor-side. In the DFIG wind turbine system, there are many factorials that affect the voltage in the DC link, such as the change of wind speed, the synchronization process of the rotor side, or the start-up process. To guarantee the safety and stability of the system, this loop must be able to adapt to the changes of both grid-side and rotor-side.

In this research, a practical control solution is proposed for the T-type converter in grid-connected mode. First, the FCS-MPC is adopted for the current control loop. With the advantage of multiple objective optimization, the FCS-MPC not only regulates the current but also can balance the neutral point voltage, reduce the switching loss, as well as reduce the common-mode voltage. Second, a fuzzy-based proportional-integral (PI) control in combination with state-machine programming is proposed to enhance the DC-link voltage regulator. This technique not only guarantees that the oscillation of the DC bus voltage is minimized but also exactly restricts the inrush current during system startup. The feasibility of the proposed approach is verified by numerical simulations where all the control algorithms are implemented by standard C-language. Hence, the consistency between simulations and practical implementations is guaranteed.

2. Grid-side converter control design

2.1. 3L T-type converter

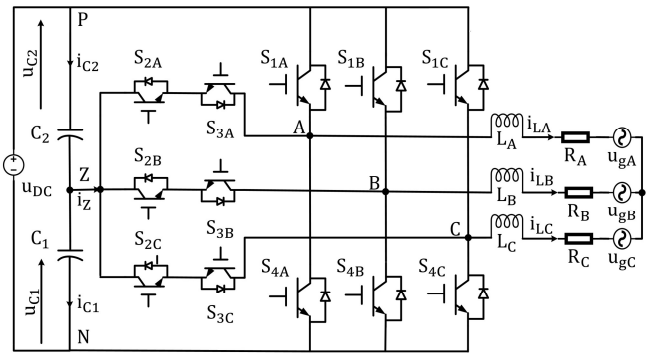

Figure 1: 3L T-type inverter circuit

The typical configuration of a 3L T-type converter is shown in Fig. 1.It is a combination between a conventional full-bridge 2L inverter and three anti-series branches of auxiliary switches to clamp the DC link neural point, which is formed by two dc-link capacitors connected in series [13]. It can be realized that each phase may have three output voltage levels P, O, N depending on the states of the main and the auxiliary switches, as provided in Table 1. Consequently, there are 27 voltage vector as depicted in Fig. 2, in which, each voltage vector can be computed by:

$$\mathbf{u}_{inv} = \frac{2}{3}(u_{AZ} + \mathbf{a}u_{BZ} + \mathbf{a^2}u_{CZ}) \tag{1}$$

In (1) $\mathbf{u}_{inv}$ is the voltage vector, $\mathbf{a} = e^{j2\pi/3}$,
u_{AZ}, u_{BZ}, u_{CZ} are the three-phase output voltage that determined by the switching state of each phase and the DC bus voltage as following:

$$u_{xZ} = S_x \frac{Vdc}{2} \tag{2}$$

where $x \in \{A, B, C\}$

Switching state	Inverter leg for each phase			
	S_1	S_2	S_3	S_4
P	1	1	0	0
O	0	1	1	0
N	0	0	1	1

Table 1: Switching states of T-type inverter

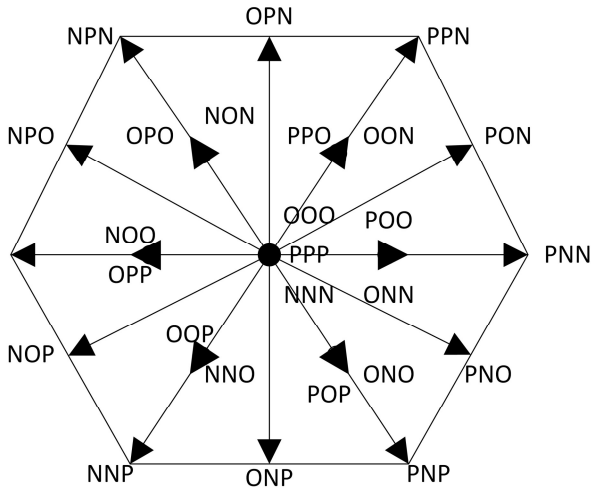

Figure 2: 27 voltage vectors output

Based on Kirchhoff's law, the relation between the grid line voltage u_g and the inverter voltage u_{inv} is:

$$\mathbf{u}_{inv} = \mathbf{u}_g + R\mathbf{i}_L + L\frac{d\mathbf{i}_L}{dt} \tag{3}$$

Where $\mathbf{u}_g = [u_{gA}, u_{gA}, u_{gA}]^T, \mathbf{i}_L = [i_{LA}, i_{LB}, i_{LC}]^T$ are the voltage and current vector, respectively. R and L are the inductor and resistor of the filter circuit.
Assuming that the DC bus voltage is constant, and the capacitors are identical ($C = C_1 = C_2$), it is possible to represent the neutral point voltage with the current and the switching states of three phase:

$$\begin{aligned}\frac{du_z}{dt} &= \frac{d(u_{c1}-u_{c2})}{dt} = \frac{-1}{C}i_z \\ &= \frac{-1}{C}((1-|S_A|)i_{LA} + (1-|S_B|)i_{LB} + (1-|S_C|)i_{LC})\end{aligned} \tag{4}$$

Using the Clarke's transform, equation (3) is rewritten in $\alpha\beta$ stationary reference frame as

$$u_{inv\alpha} = u_{g\alpha} + Ri_{L\alpha} + L\frac{di_{L\alpha}}{dt} \tag{5}$$

$$u_{inv\beta} = u_{g\beta} + Ri_{L\beta} + L\frac{di_{L\beta}}{dt} \tag{6}$$

Equation (5) and (6) can be rewritten as:

$$\begin{bmatrix} u_{inv\alpha} \\ u_{inv\beta} \end{bmatrix} = \begin{bmatrix} u_{g\alpha} \\ u_{g\beta} \end{bmatrix} + R\begin{bmatrix} i_{L\alpha} \\ i_{L\beta} \end{bmatrix} + L\frac{d}{dt}\begin{bmatrix} i_{L\alpha} \\ i_{L\beta} \end{bmatrix} \tag{7}$$

2.2. Model predictive control

The block diagram of the 3L T-type converter control system is shown in Fig.3. The inner loop is the current regulator, in which FCS-MPC is employed. To conduct the control design, the continuous-time model (4) and (7) need to be discretized as following.
Applying the Backward Euler discretization to (7), it gives:

$$\frac{L+RT_s}{L}\begin{bmatrix} i_{L\alpha,k+1} \\ i_{L\beta,k+1} \end{bmatrix} = \frac{T_s}{L}\begin{bmatrix} u_{inv\alpha,k+1} - u_{g\alpha,k+1} \\ u_{inv\beta,k+1} - u_{g\beta,k+1} \end{bmatrix} + \begin{bmatrix} i_{L\alpha,k} \\ i_{L\beta,k} \end{bmatrix} \tag{8}$$

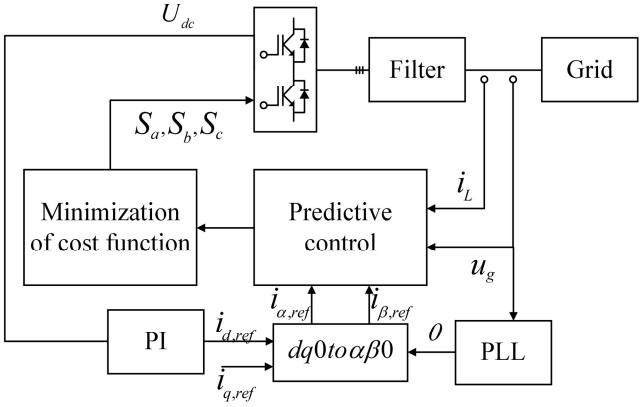

Figure 3: Block diagram of the proposed control scheme

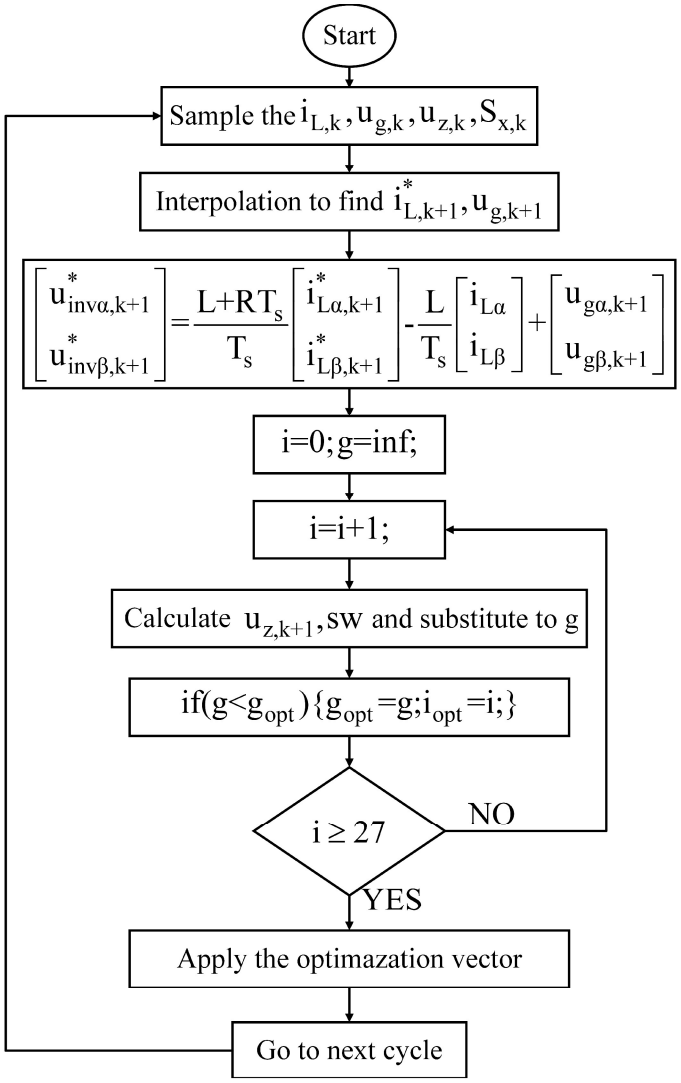

Figure 4: Flowchart of MPC algorithm

In (8), by substituting the predictive current $i_{L\alpha,k+1}, i_{L\beta,k+1}$ by their reference values $i^*_{L\alpha,k+1}, i^*_{L\beta,k+1}$, the control output voltage is :

$$\begin{bmatrix} u^*_{inv\alpha,k+1} \\ u^*_{inv\beta,k+1} \end{bmatrix} = \frac{L+RT_s}{T_s}\begin{bmatrix} i^*_{L\alpha,k+1} \\ i^*_{L\beta,k+1} \end{bmatrix} - \frac{L}{T_s}\begin{bmatrix} i_{L\alpha,k} \\ i_{L\beta,k} \end{bmatrix} + \begin{bmatrix} u_{g\alpha,k+1} \\ u_{g\beta,k+1} \end{bmatrix} \tag{9}$$

The reference current is computed by the outer loop controller and its predictive values can be achieved by using the second

order Lagrange extrapolation [14]:

$$\begin{bmatrix} i^*_{L\alpha,k+1} \\ i^*_{L\beta,k+1} \end{bmatrix} = 3\begin{bmatrix} i^*_{L\alpha,k} \\ i^*_{L\beta,k} \end{bmatrix} - 3\begin{bmatrix} i^*_{L\alpha,k-1} \\ i^*_{L\beta,k-1} \end{bmatrix} + \begin{bmatrix} i^*_{L\alpha,k-2} \\ i^*_{L\beta,k-2} \end{bmatrix} \tag{10}$$

The extrapolation can also be applied to grid voltage similarly, and results in:

$$\begin{bmatrix} u_{g\alpha,k+1} \\ u_{g\beta,k+1} \end{bmatrix} = 3\begin{bmatrix} u_{g\alpha,k} \\ u_{g\beta,k} \end{bmatrix} - 3\begin{bmatrix} u_{g\alpha,k-1} \\ u_{g\beta,k-1} \end{bmatrix} + \begin{bmatrix} u_{g\alpha,k-2} \\ u_{g\beta,k-2} \end{bmatrix} \tag{11}$$

The discrete time version of (4) can also be obtained in a similar manner and expressed by:

$$\begin{aligned} u_{z,k+1} = u_{z,k} &+ \frac{T_s}{2C}(2|S_{A,k+1}| - |S_{B,k+1}| - |S_{C,k+1}|)i_{L\alpha,k} \\ &+ \frac{\sqrt{3}T_s}{2C}(|S_{B,k+1}| - |S_{C,k+1}|)i_{L\beta,k} \end{aligned} \tag{12}$$

In addition to the main control goal which minimizes the current tracking error, the inner loop must also control the neutral point voltage and reduce the switching frequency of the converter. Hence, the cost function is as follow:

$$\begin{aligned} g = &|u^*_{inv\alpha,k+1} - u_{inv\alpha,k+1}| + |u^*_{inv\beta,k+1} - u_{inv\beta,k+1}| \\ &+ \lambda_{dc}|u_{z,k+1}| + \lambda_n sw \end{aligned} \tag{13}$$

In (13), $sw = |S_{x,k+1} - S_{x,k}|$, and λ_{dc}, λ_n are the weighting factors that can be used to adjust the capacitor voltage balancing and the switching loss, respectively.
In every consecutive sampling cycle, the voltage vector which minimizes the cost function (13) is obtained by using the flowchart shown in Fig.4.

2.3. Conventional DC bus voltage control design

Suppose that the equivalent serial resistance (ESR) of the dc-bus capacitor is sufficient small, the energy E_c stored in the capacitor is:

$$E_c = \frac{1}{2}Cv^2_{dc} \tag{14}$$

The time derivative of this energy must be equal to the power transfer between the grid and the load, which means:

$$\frac{1}{2}C\frac{dv^2_{dc}}{dt} = P_g - P_{load} \tag{15}$$

It can be seen that (15) is nonlinear with v_{dc}. To make (15) linear, choose the new state variable $W = v^2_{dc}$,then it gives:

$$\frac{1}{2}C\frac{dW}{dt} = P_g - P_{load} \tag{16}$$

Define R_{load} as the equivalent load of the DC side, then P_{load} can be computed by:

$$P_{load} = \frac{v^2_{dc}}{R_{load}} = \frac{W}{R_{load}} \tag{17}$$

In practice, it is impossible to determine R_{load} depends on the working condition of the DFIG, e.g., the wind speed. However, the bound of R_{load} can be roughly obtained based on the rated power P_{rated} and the efficiency η of the converter as following:

$$\frac{v^2_{dc,rated}}{P_{rated}} \le R_{load} \le \frac{v^2_{dc,rated}}{P_{loss}} \tag{18}$$

The instantaneous power on the grid side is calculated by

$$P_g = \frac{3}{2}E_g i_d \tag{19}$$

In which, i_d is the amplitude of the sinusoidal grid-connected current, also the d-axis current in voltage-oriented control (VOC) reference frame, and E_g is the grid phase voltage amplitude.
Substituting (17) and (19) into (16), it yields:

$$\frac{1}{2}C\frac{dW}{dt} = \frac{3}{2}E_g i_d - \frac{W}{R_{load}} \tag{20}$$

Based on (20), the transfer function which shows the relation between the input i_d and the output W in discrete-time domain is:

$$\frac{W_k}{i_{d,k}} = \frac{\frac{3E_gT_s}{C}z^{-1}}{1-(1-\frac{2T_s}{R_{load}C})z^{-1}} \tag{21}$$

Where T_s is the sampling time. To regulate the dc-bus voltage represented by (2), a conventional proportional-integral (PI) as described by (22) is sufficient.

$$W_{PI} = K_P\frac{1-Dz^{-1}}{1-z^{-1}} \tag{22}$$

In which, $D = 1 - \frac{T_s}{T_I}$ with T_I is the integral time constant. From (21) and (22), the closed-loop transfer function of the dc voltage control loop is:

$$W_{CL} = \frac{b_1K_Pz^{-1} - b_1K_PDz^{-2}}{1+(b_1K_P-a_1)z^{-1}+(a_1-b_1K_PD)z^{-2}} \tag{23}$$

with $b_1 = \frac{3E_g}{T_s}$ and $a_1 = 1 - \frac{2T_s}{R_{load}C}$.Theoretically, the integral time T_I should be chosen such that pole-zero cancellation occurs in (23) , which means:

$$T_I = \frac{R_{load}C}{2} \tag{24}$$

Then, (23) is reduced order and represented by:

$$W_{CL} = \frac{3T_sK_PE_gz^{-1}}{C(1-z^{-1})+3T_sK_PE_gz^{-1}} \tag{25}$$

Equation (25) shows that, once the pole-placement occurs, the dynamic of the closed-loop system mainly governed by the proportional gain K_P. Larger K_P may improve the transient response. However, it can be seen from (24) that T_I cannot be chosen as a constant since it is load dependent, which means pole-zero cancellation is impossible in practice. Hence, a practical approach is proposed in this research to handle the dc voltage control loop as following.

2.4. The proposed DC bus controller

For such a high-power system as DFIG, the capacity of the dc-bus capacitor is huge. Therefore, limiting the inrush current and quickly suppressing the dc voltage oscillation is extremely important to the startup process. To deal with this issue, the startup of the grid-side converter is divided into three states as following.

In the first state, the converter takes power from the grid to charge the dc-link capacitor via a serial resistor and the diode, all the control loops are not active. When the dc voltage reaches the stable value of the diode rectifier, the serial resistor is bypassed and the system switches to state 2.
In the second state, the dual-loop control system is activated to boost the voltage to its higher desired value. Even though, the rotor side converter of the DFIG is inactive, which means the equivalent load $R_{load} \approx \infty$,following that (21) can be regarded as a pure integrator. As a result, a proportional controller is sufficient to bring the dc voltage to its desired value without overshoot. The point is how to choose the proportional gain K_P to limit the inrush current.
Suppose that the stable value of the diode rectifier is V_m and the set-point of the dc-bus voltage is V^*. Then, the maximal tracking error since the control system is activated is:

$$E_{Max} = V^{*2} - V_m^2 \tag{26}$$

It can easily be realized that the current used to boost the capacitor voltage is maximum at this instance. Since the proportional controller is adopted, the maximum reference current is computed by:

$$I_{d,Max}^* = K_P E_{Max} \tag{27}$$

From (27), it can be deduced that the amplitude of the inrush current can be exactly limited by selecting K_P as following:

$$K_P = \frac{I_{d,Max}^*}{E_{Max}} \tag{28}$$

With K_P computed by (28), the dc voltage reaches its set-point asymptotically. When the dc voltage approaches the vicinity of the set-point, the system switches to state 3
In the third state, the rotor-side converter is enabled which means $R_{load} \neq 0$ and the fuzzy-based PI controller is activated to adjust both K_P and T_I simultaneously. The fuzzy tuning is based on the following observations:

- The integral time constant T_I helps compensate the tracking error but may cause oscillation in the transient state if too small. Hence, T_I should be kept large in steady-state, and only bc rcducd as thc tracking crror incrcasc.Thc bound of T_I is obtained based on (18) and (24):

$$\frac{Cv_{dc,rated}^2}{P_{rated}} \leq T_I \leq \frac{Cv_{dc,rated}^2}{P_{loss}} \tag{29}$$

- A large proportional gain K_P gives large control signal to quickly compensate the tracking error in transient state. In steady state, K_P can be kept small to increase the stability margin of the control system. The bound of K_P be roughly obtained based on (28):

$$\frac{\eta I_{rated}}{E_{Max}} \leq K_P \leq \frac{I_{rated}}{E_{Max}} \tag{30}$$

  Equation (30) means that in the worst case where the maximum tracking error exists, the controller is not saturated by the proportional term.

To implement the above-mentioned tuning rules, Mamdani fuzzy with triangle membership function (MF) is chosen. The input of the fuzzy-based PI controller is the absolute of the tracking error, and the outputs are K_P and T_I. Each MF is composed of five grades: PZ, PS, PM, PL, PH, corresponding to Zero, Small Positive, Medium Positive, Large Positive, and Huge Positive. The details of MFs are shown in Fig. 5, Fig. 6 and Fig. 7. The triangle membership function is described by:

$$\mu(x,L,C,R) = \begin{cases} \frac{x-L}{C-L} & if L \leq x \leq C \\ \frac{R-x}{R-C} & if C \leq x \leq R \\ 0 & otherwise \end{cases} \tag{31}$$

Where (L, R, C) stands for leftmost point, rightmost point, and central point.

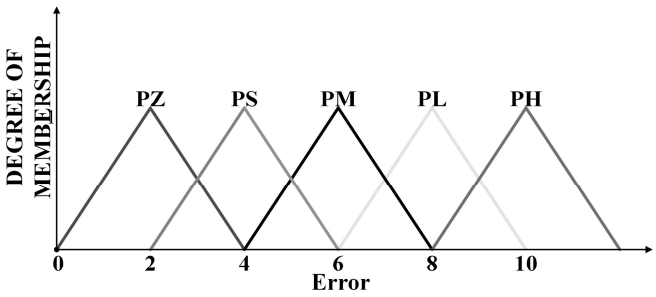

Figure 5: Input membership function

The fuzzy rules are as follows:
If $|e(t)| = PZ$ then $T_I = PH$ and $K_P = PZ$
If $|e(t)| = PS$ then $T_I = PL$ and $K_P = PS$
If $|e(t)| = PM$ then $T_I = PM$ and $K_P = PM$
If $|e(t)| = PL$ then $T_I = PS$ and $K_P = PL$
If $|e(t)| = PH$ then $T_I = PZ$ and $K_P = PH$

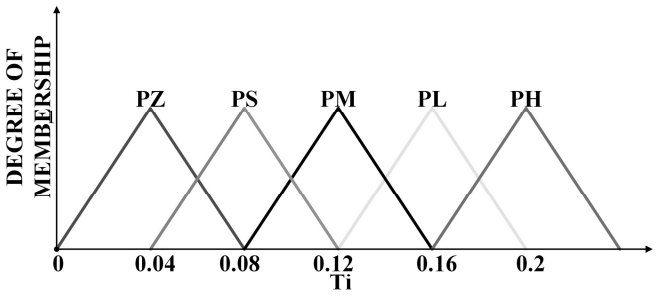

Figure 6: Output membership function of T_I

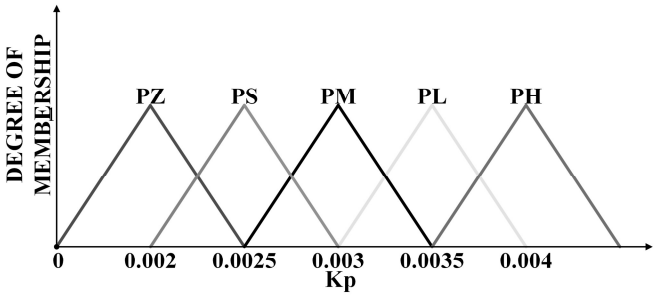

Figure 7: Output membership function of K_P

The fuzzy interference control rules are generated using max-min method. The center of gravity method has been selected to calculate the crisp value of output. The general equation of

this method is:

$$y_o = \frac{\int y\mu_{R(y)}dy}{\int \mu_{R(y)}dy} \tag{32}$$

In which, $\mu_R(y)$ is the output fuzzy set after the max-min method is applied, and y is a variable of this set.

3. Simulation and result

To verify the feasibility and the effectiveness of the proposed controller, a numerical simulation is conducted where basic parameters are provided in Table 2.

L	3mH
R	0.1Ω
C1,C2	3000μ F
f_g	50Hz
P	60kW
λ_{dc}	20
λ_n	60
$V_{g,peak}$	391V
V_{dc}	950V

Table 2: System parameters

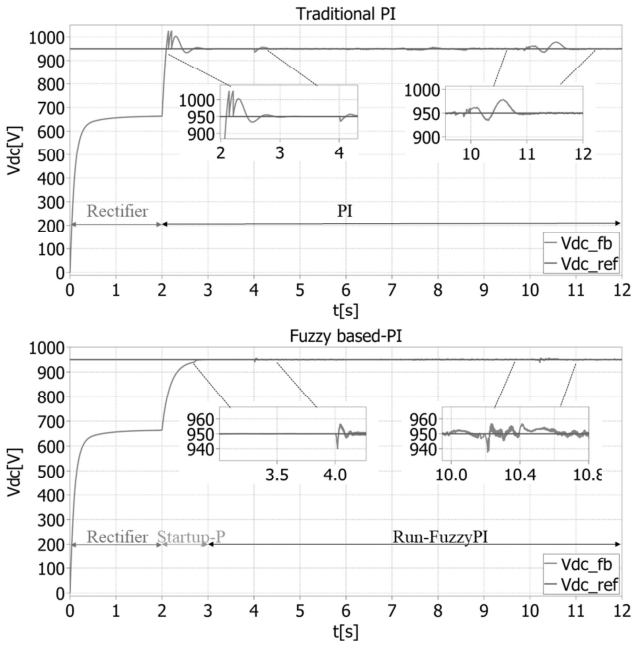

Figure 8: DC link voltage

Fig. 8 shows the comparative tracking performance between the proposed controller and a conventional PI controller. It can be clearly seen that with fixed parameters, the conventional PI causes a larger dc-voltage overshoot, although the transient-time is almost the same. The proposed controller with a strict startup procedure and parameters adjusted according to load condition gives a much better response where the overshoot and the fluctuation of the dc voltage are minimized. The K_P, T_I factors which is computed by the fuzzy-based PI controller is shown in Fig.9 .

In the first two seconds, a serial power resistor is used to limit the inrush current that charges the capacitor. At time instance 2s, the control system is activated to boost the dc voltage to its desired value. With the proportional voltage controller where K_P is computed by (28), the dc voltage approaches its setpoint asymptotically without overshoot, whilst the inrush current

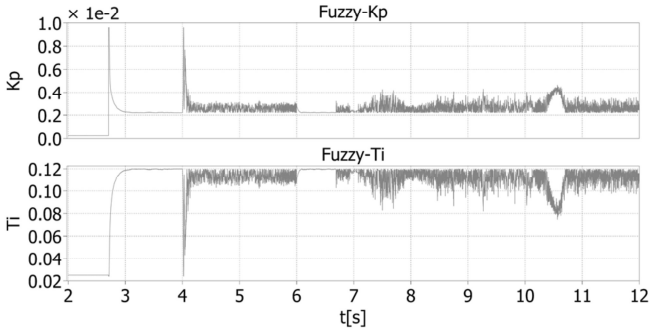

Figure 9: Variation Kp, Ti according to fuzzy tuning

amplitude is exactly limited, i.e., 100A as illustrated in Fig. 10. From the 3rd second forwards, the fuzzy-based PI controller is activated, and the rotor side converter is connected to the grid one second later. It can be observed that the controller takes less than 0.1s to stabilize the DC voltage with negligible overshoot. Even when the power transfer is suddenly changed, i.e., at time instance 7 and 10, fluctuations in the dc voltage are barely observable.

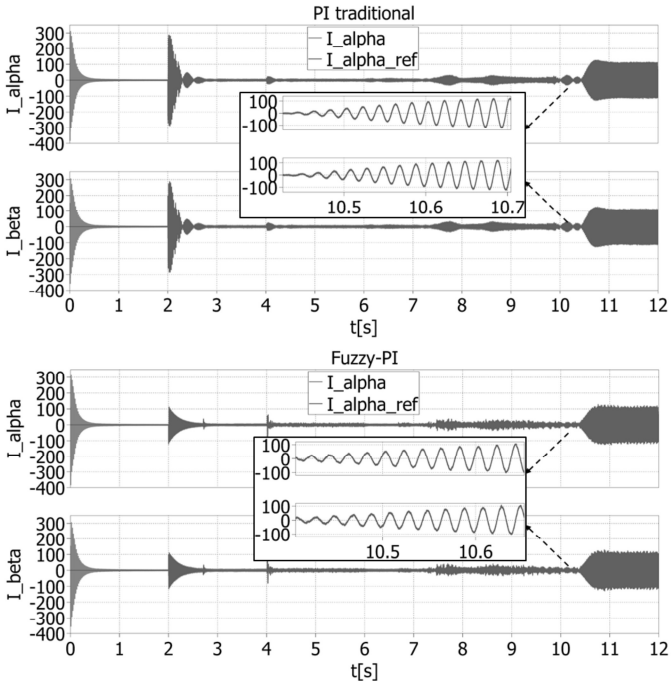

Figure 10: Alpha-beta inject current

Fig.11 shows the THD of grid current with and without the switching frequency reduction coefficient λ_n. Without λ_n, the THD of the current is lower, i.e., 2,32% in comparison with 2,78%. However, the average switching frequency once the λ_n is used is 5810Hz which is 18% lesser than when the λ_n is

unused.

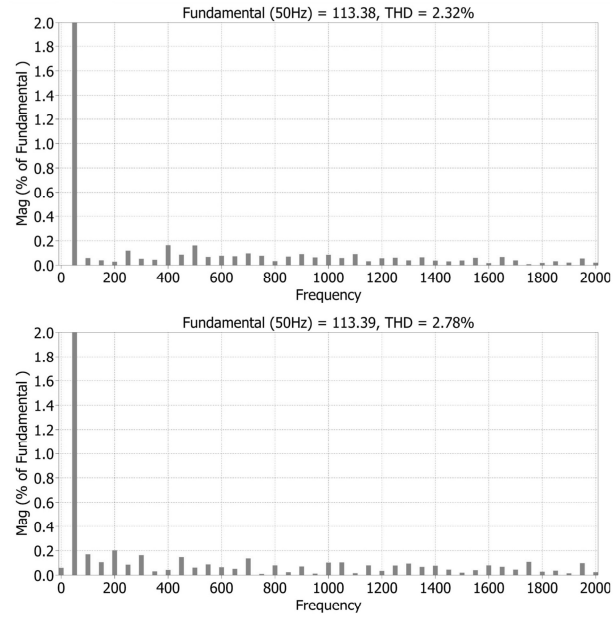

Figure 11: THD of the grid current without λ_n and with λ_n

Figures 12 and 13 show the power transfer and the dc-link capacitor voltage, respectively. It can be seen that in addition to ensuring the minimal grid-connected current tracking error, the MPC can also maintain the dc-link capacitor voltage balance in both light and heavy load conditions thanks to its multi-objective optimization ability.

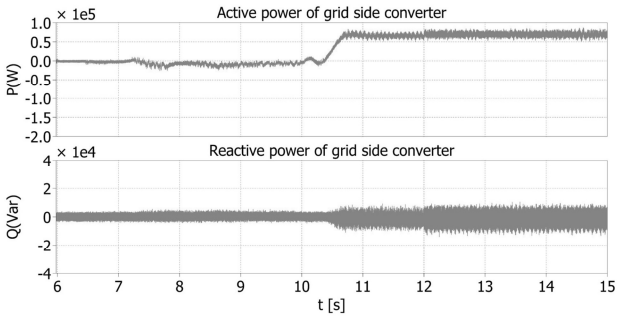

Figure 12: Inject active and reactive power

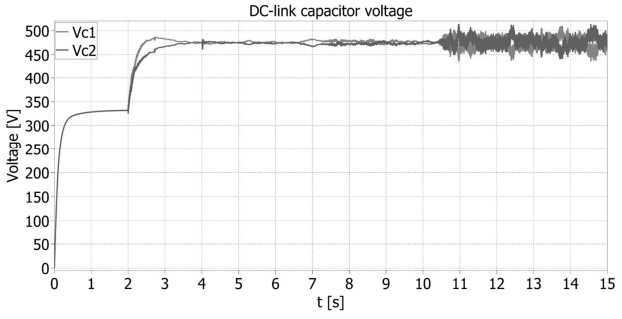

Figure 13: Voltage on DC link capacitors

4. Conclusion

This research presents an approach to control the grid side converter of a DFIG used for wind power system. First, the T-type topology which have many outstanding advantages over the conventional three phase-three leg topology is employed. Then, a various control techniques are adopted to improve the performance of the control system such as FCS-MPC and fuzzy-based PI controller. The FCS-MPC is used not only to regulate the grid-connected current but also to reduce the switching frequency and balancing the neutral point voltage. For the dc-bus voltage control loop, a fuzzy-based PI controller is proposed to quickly suppress the voltage oscillation with minimal overshoot. Specifically, a strict procedure is proposed to guarantee the safe startup of such high-power systems like DFIG, in which not only inrush current is exactly limited but also the voltage overshoot is eliminated. Numerical simulation results show that the proposed strategy can guarantee the stability and sustainability of the control system. In addition, the feasibility of the control system is also ensured since the algorithm is implemented by standard C-language, which can easily be utilized by any digital control platform.

Acknowledgement

This research is funded by the Hanoi University of Science and Technology (HUST) under project number T2020-SAHEP-004.

References

[1] Ulu, Cenk and KÖMÜRGÖZ, Güven, (2017) *Electrical design and testing of a 500 kW doubly fed induction generator for wind power applications.* Turkish Joural Of Electrical Engineering & Computer Sciences

[2] Dida, Abdelhak and ben attous, Djilani, (2016) *A complete modeling and simulation of DFIG based wind turbine system using fuzzy logic control* Frontiers in Energy

[3] Demirbaş, Şevki and Bayhan, Sertaç, (2011) *Grid synchronization of doubly fed induction generator in wind power systems* Frontiers in Energy 2011 International Conference on Power Engineering, Energy and Electrical Drives

[4] Arbi, Jihen and Ghorbal, Manel Jebali-Ben and Slama-Belkhodja, Ilhem and Charaabi, Lotfi, (2009) *Direct Virtual Torque Control for Doubly Fed Induction Generator Grid Connection* IEEE Transactions on Industrial Electronics

[5] Hughes, F.M. and Anaya-Lara, O. and Jenkins, N. and Strbac, G., (2005) *Control of DFIG-based wind generation for power network support* IEEE Transactions on Power Systems

[6] Tamalouzt, Salah and Belkhier, Youcef and Sahri, Younes and Bajaj, Mohit and Ullah, Nasim and Chowdhury, Md. Shahariar and Titseesang, Teerawet and Techato, Kuaanan, (2021) *Enhanced Direct Reactive Power Control-Based Multi-Level Inverter for DFIG Wind System under Variable Speeds* Sustainability

[7] Alaa M. Al-Quteimat, (2018) *Control layout of doubly fed induction generator with respect to low voltage ride through for wind energy conversion system*

[8] Vo, Dai-Van and Nguyen, Minh-Khai and Do, Duc-Tri and Choi, Youn-Ok, (2019) *CA Single-Phase Nine-Level Boost Inverter* Energies

[9] Suraj J. Raiyani, Ravindra Gamit, Balvant Solanki and G. Pradeepa *A Technological Review: On Cascaded H-Bridge Multilevel Inverters* International Journal for Innovative Research in Science & Technology

[10] Prathiba, T and Renuga, P, (2012) *A comparative study of total harmonic distortion in multi level inverter topologies* Journal of Information Engineering and Applications

[11] Pho, Bao Binh and Tran, Trong Minh and Nguyen, Manh Linh and Hoang, Phuong Vu, (2020) *Discrete-Time Quasi Sliding Mode Control of Single-phase T-type Inverters for Residential PV Applications* 2020 International Conference on Advanced Mechatronic Systems (ICAMechS)

[12] Tsili, M and Papathanassiou, S, (2009) *IET Renewable Power Gener*

[13] Salem, Aboubakr and Abido, Mohammed, (2018) *T-Type Multilevel Converter Topologies: A Comprehensive Review* Arabian Journal for Science and Engineering

[14] Xing, Xiangyang and Chen, Alian and Zhang, Zicheng and Chen, Jie and Zhang, Chenghui, (2016) *Model predictive control method to reduce common-mode voltage and balance the neutral-point voltage in three-level T-type inverter* 2016 IEEE Applied Power Electronics Conference and Exposition (APEC)

[15] Phuong Vu, Anh Tuan Do, Linh Nguyen, *A novel Multi-step Model Predictive Control design for three-phase T-Type inverter in grid-connected mode* International Journal of Renewable Energy Research (IJRER), Vol 11, No 4 (2021)

[16] Manh Linh NGUYEN, Phuong VU, *Advanced single-loop discrete-time control for T-type voltage source inverter with minimum capacitor voltage ripple modulation* Turkish Journal of Electrical Engineering & Computer Sciences, Year: 2021 Volume: 29 Number: 7

[17] Phuong Vu, Trang Van Nguyen, Manh Dinh Nguyen, Cuong Ngoc Tran, Anh Tuan Do, *Modified Space Vector Modulation Technique for Three Phase Three Level T-type Inverter* International Journal of Renewable Energy Research (IJRER), Vol 11, No 3 (2021)

[18] D. A. Tuan, P. Vu, and N. V. Lien, *Design and Control of a Three-Phase T-Type Inverter using Reverse-Blocking IGBTs* Eng. Technol. Appl. Sci. Res., vol. 11, no. 1, pp. 6614–6619, Feb. 2021